A Computational Framework for Fluid Structure Interaction in Biologically Inspired Flapping Flight

David J. Willis *, Emily R. Israeli †, Per-Olof Persson ‡, Mark Drela §, Jaime Peraire ¶,
Sharon M. Swartz ‖, Kenneth S. Breuer **

Although there are many examples of successful flapping flight in nature, engineers and scientists have had difficulty achieving high performance levels using flapping wing designs. In this paper a computational framework to design and analyze flapping flight for Micro Aerial Vehicle size scales is presented. This computational framework exploits a series of different geometric and physical fidelity level representations. The tools considered are wake only methods(HallOpt), lifting line methods(ASWING), panel methods (FastAero) and high order discontinuous Galerkin methods for solving the Navier Stokes equations(3DG). Using this suite of tools, both design oriented explorations as well as analysis of animal flight can be performed. In this paper we present the framework in its current state and illustrate its use by examining several characteristic problems.

Nomenclature

Γ	Circulation
ϕ	Scalar Potential, satisfies potential flow equations
λ	Lagrange Multiplier
c	chord
$\vec{F}_1$	First order force
AIC	Aerodynamic Influence Coefficients Matrix
RHS	RHS Vector
C_L	Three Dimensional Lift coefficient, $C_L = \frac{L}{\frac{1}{2}\rho U^2 S}$
C_T	Three Dimensional Thrust Coefficient, $C_T = \frac{T}{\frac{1}{2}\rho U^2 S}$
C_P	Three Dimensional Thrust Coefficient, $C_P = \frac{P}{\frac{1}{2}\rho U^3 S}$
C_l	Two Dimensional Lift coefficient, $C_l = \frac{l}{\frac{1}{2}\rho U^2 c}$
C_t	Two Dimensional Thrust Coefficient, $C_t = \frac{t}{\frac{1}{2}\rho U^2 c}$
C_p	Two Dimensional power coefficient, $C_p = \frac{p}{\frac{1}{2}\rho U^3 c}$
M	Moment
L	Lift
D	Drag
θ	Airfoil orientation
η	Efficiency (ratio of power in to power out)
ω_r	Reduced frequency, $\omega_r = \frac{\omega c}{2U}$
St	Strouhal Number, $St = \frac{fA}{U}$
$\vec{U}$	Freestream Velocity

*Research Scientist, Department of Aeronautics and Astronautics, MIT
†Graduate Student, Department of Aeronautics and Astronautics, MIT
‡Instructor, Department of Mathematics and Statistics, MIT
§Professor, Department of Aeronautics and Astronautics, MIT
¶Professor, Department of Aeronautics and Astronautics, MIT
‖Associate Professor, Department of Ecology and Evolutionary Biology, Brown University.
**Professor, Division of Engineering, Brown University.

U	Magnitude of the Freestream Velocity
$\vec{V}$	Velocity Relative to the Wing
C_{spring}	Spring Constant
$I_{L.E.}$	Mass moment of inertia of an airfoil about the leading edge
x_{cg}	The location of the airfoil c.g. with respect to the leading edge

Subscript

1	First Order
prop	Propulsive

I. Introduction

While Micro Aerial Vehicle (MAVs) flight suffers from the unpredictable characteristics of transitional and low Reynolds number flight, birds and bats have proven platforms with inherent design features capable of combating or overcoming these adverse flow conditions. One possible key to nature's success is that birds and bats use active morphing as well as passive compliance in order to achieve flight.[1,2] Although these active morphing winged animals are complex biological systems, their wings and kinematics are likely tuned, to a certain extent, for achieving efficient flight and aerodynamics. Furthermore, it is likely that these animals exploit beneficial shape changes due to passive fluid structure interaction where possible. To further support these hypotheses, the evolutionary process of flying animals exhibits significant skeletal structure adaptations such as, large material property gradients and variations,[1,3,4] the development of extreme adaptations (bats wings are essentially equivalent to hands,[4] birds feathers are believed to be adaptations of scales[1]), the development of advanced respiratory system strategies (birds lungs[1]), the fusing of bones in birds,[1] as well as the complete loss of certain traditional skeletal features (such as several fingers in birds). Although observing and gaining inspiration from these animals can provide significant insight into the physical requirements of flapping flight, it remains an engineering challenge to develop equivalently effective flapping wing vehicles. These animals do not provide the scientist and engineer with the ability or flexibility to explore the flapping flight design space outside of the normal operating parameters of these animals, making it difficult to separate biological system constraints from the design process. Furthermore, the limits of efficiency, performance and maneuverability of these animals may rest in biological constraints, therefore, making them an effective, but perhaps not perfect model for engineered systems. Using computational tools in combination with live animal research, theory and experiment, provides a compelling approach to assess the natural flapping flight design space as well as the surrounding design space. In this paper, several computational tools are presented as a synergistic framework to better understand the physics of flapping flight.

Computational fluid dynamics tools have been used in many diverse studies of flapping flight as well as flapping foil propulsion.[5–8] In this paper we break from the traditional single computational tool strategy and propose a multi-fidelity series of tools which can be effective in understanding flapping flight physics. Due to the expansive nature of the flapping flight parameter design space, we propose a strategy similar to that used in air vehicle design, namely a series of multiple-fidelity physics and geometry computational tools capable of capturing the trends of the particular problem under investigation. The fluid dynamics tools, which lie at the center of the toolset include:

- **HallOpt** : A wake only tool used to determine the minimum power vorticity distribution in a flappers' wake.
- **ASWING** : A coupled lifting line, nonlinear beam structures, and controls aircraft analysis and design tool.
- **FastAero** : An unsteady boundary element method, potential flow solver (panel method).
- **3DG** : A high order, discontinuous Galerkin solution methodology for the solution of the Navier Stokes Equations.

Although several of the tools are still undergoing development (at some level), the current capability and methodology is illustrative of the multi-fidelity strategy under consideration. By using a multi-fidelity approach, design and analysis can be performed at an appropriate level of fidelity, in a moderate amount of

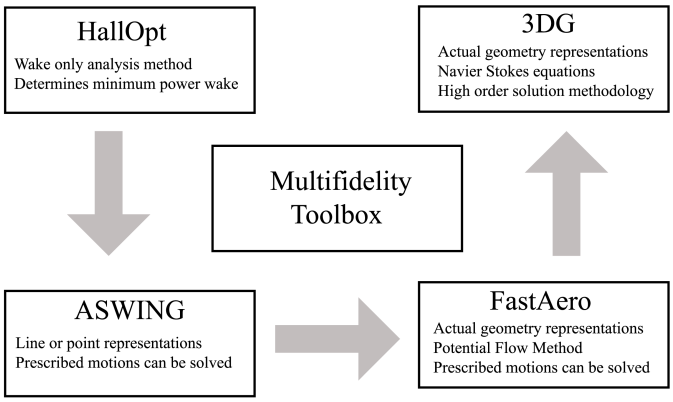

Figure 1. An illustration of the multiple fidelity computational methods being investigated for analyzing flapping flight.

time. For example, the main feature of flapping wing locomotion is to generate a time dependent vorticity distribution in the wake of the vehicle. Although generating the exact wake vorticity distribution requires a high fidelity geometry representation as well as a high fidelity physics modeling tool, it is possible that an approximation of that wake vorticity may be sufficient to explain certain characteristics observed in efficient flapping flight such as the advance ratio,[9] or the Strouhal number.[12]

II. Multi-fidelity Methods

The computational framework which is presented in this paper is illustrated in figure 1. The overall goal of the framework is to reduce the computational complexity of parameter selection while capturing the essential trends of the flapping wing system. In the sections which follow, a description of the salient features of each of the computational approaches is presented along with the various limiting assumptions which appear in the analysis.

II.A. Wake Only Method: *HallOpt*

HallOpt is a wake only method which was developed[9–11] for the analysis of flapping vehicles. The wake of a lift-generating object passing can indicate the history of the forces which the body exerts on the fluid and visa versa. In effect, the wake vorticity pattern is much like a footprint. Wake only analysis methods based on vortex lines or lattices are powerful, while also remaining a simple and cost effective method for computing the desired characteristics of a flight vehicle. Two well known analysis approaches are the Trefftz Plane induced drag computation for finite wings[15] and the Betz criterion propeller analysis. The *HallOpt* method is no different than these traditional wake only methods, in that it can be used to determine the minimum power wake circulation distribution for a given set of desired time averaged, first order forces.

II.A.1. The Wake Only Method For Wake Geometries

In the method of Hall et al[9–11] the wake shed by a flapping vehicle is assumed to be infinitely periodic in the flight direction. A single period of this wake is selected and the optimal circulation distribution for that particular wake is determined. The following steps, combined with figure 2, highlight the general solution process:

- A single period of the wake surface formed by the trailing edge trace is defined.
- The wake shape is discretized using a discrete vortex lattice.[18]
- First order force constraints and viscous drag polar details are expressed as functions of the yet unknown wake vorticity. See equation 1.

- The minimum total power vorticity distribution is expressed as a constrained quadratic optimization problem whose minimum is simply found by solving a linear system.

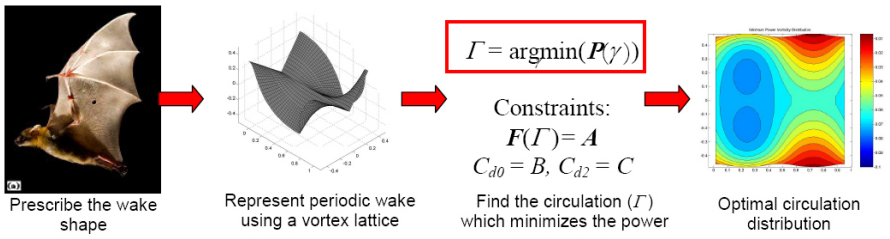

Figure 2. A pictorial representation of the HallOpt solution process. The first step in the process is to determine the wake shape under consideration. Here a bat (photo: Arnold Song, Brown University) is shown as a possible example. The wake trace is then discretized using a vortex lattice representation. A minimization problem is then posed to determine the vorticity distribution which minimizes the power, subject to force constraints. The final image in the sequence shows a minimum power wake circulation distribution from above (flapper flying from left to right, starting with the downstroke, blue represents high lift producing circulation, while red represents regions of lower circulation).

II.A.2. Wake Only: Accounting for Forces

The generation of forces can be related to the circulation distribution and the shape of the wake. The first order, time averaged forces from a given wake are:

$$\vec{F}_1 = \frac{\rho}{T}\int_{WS} \Gamma \cdot \hat{n} dS_{WS} \tag{1}$$

Note, that in the computation of the thrust and lift forces, there is no accounting for the induced velocity due to the vorticity in the wake. The ability to approximately compute and balance the prescribed periodic-averaged thrust forces with the induced and viscous drag is possible, and has been investigated as an option in HallOpt, permitting complete balance of flight forces to be satisfied if desired.

II.A.3. Wake Only: Accounting for Power

The power required to create the particular wake vorticity distribution is composed of an induced power contribution (related to the vorticity induced losses) and a viscous contribution (due to the viscosity in the fluid which can be related to the circulation distribution in the wake using a quasi-steady drag polar approximation.[10]):

$$P = -\frac{\rho}{2T}\int_{WS} \Delta\phi \nabla\phi \cdot \hat{n}\, dS + \frac{\rho}{2T}\int_{WS}\left(\frac{4C_{d2}}{c}\right)(\Gamma - \Gamma_0)^2 dS + \frac{\rho}{2T}\int_{WS}(U^2 c\, C_{d0}) \cdot \left(\frac{ds}{dx}\right)^2 dS \tag{2}$$

To determine the wake circulation which minimizes the power in the wake, the constrained optimization problem is solved. The force constraints are added to the relationship for the power through a series of Lagrange multipliers. The quadratic functional representing the power can be minimized by solving a linear system as illustrated in the original reference.[9] The resulting circulation distribution, Γ, is that which minimizes the power.

II.B. Lifting Line Method: *ASWING*

ASWING[14] is a dynamical simulation tool for highly flexible aircraft. Its overall model consists of four coupled sub-models (Structural, Aerodynamic, Flight-dynamics, Control), each described below together with its state variables and equations. Accompanying the description is a pictorial representation (Figure 3).

II.B.1. Structural model

This consists of nonuniform nonlinear connected beams, which allow arbitrarily large deflections, with arbitrary loads. Twelve unsteady state variables and associated equations are defined versus a span-wise coordinate s:

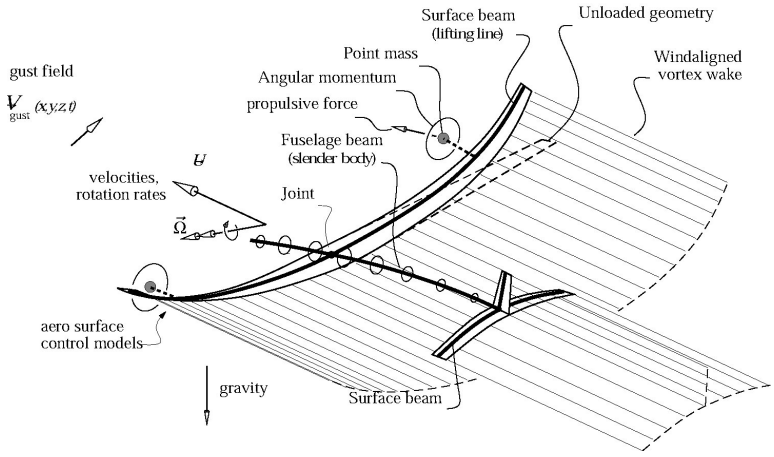

Figure 3. A pictorial representation of the ASWING solution method. The figure illustrates the different components of the solution method.

$\vec{r}_{(s,t)}$,	$\frac{\partial \vec{r}}{\partial s} = f(\vec{\theta} \ldots)$	beam locations, position/angle displacement relations
$\vec{\theta}_{(s,t)}$,	$\frac{\partial \vec{\theta}}{\partial s} = f(\vec{M} \ldots)$	beam Euler angles, curvature/moment relations
$\vec{M}_{(s,t)}$,	$\frac{\partial \vec{M}}{\partial s} = f(\vec{F}, \frac{\partial \vec{\theta}}{\partial t} \ldots)$	beam moment resultants, moment-equilibrium relations
$\vec{F}_{(s,t)}$,	$\frac{\partial \vec{F}}{\partial s} = f(\rho V \Gamma, \frac{\partial \vec{r}}{\partial t} \ldots)$	beam force resultants, force-equilibrium relations

Two types of beams are used: *surface beams* and *fuselage beams*. They have identical structural representations, but different aerodynamic representations and hence different applied aerodynamic loads.

II.B.2. Aerodynamic model

This consists of a lifting line with circulation and trailing vorticity on each surface beam, and a slender body with source and doublet strengths for each fuselage beam. One unsteady state variable and associated equation is defined along a surface beam:

$\Gamma_{(s,t)}$,	$\vec{V} \cdot \hat{n} + kc\frac{\partial \Gamma}{\partial t} = 0$	circulation, flow tangency

The local beam-relative velocity $\vec{V}$ depends on the aircraft velocity $\vec{U}$, rotation rate $\vec{\Omega}$, and also on all the circulation distributions on all the beams and its trailing vorticity. The latter is computed via a Weissinger-type vortex lattice approach. The $\frac{\partial \Gamma}{\partial t} = 0$ term approximately captures the assumed-local contribution of unsteady vortex shedding. The local normal vector $\hat{n}$ depends on the deformed beam geometry and control deflections $\vec{\delta}$.

II.B.3. Flight-dynamics model

This is the standard aircraft flight dynamics model, but with time-dependent inertias due to the deforming geometry. The following state variables and equations are used:

$\vec{R}_{(t)}$,	$\frac{d\vec{R}}{dt} = f(\vec{U}, \vec{\Theta})$	aircraft location, position/velocity relations
$\vec{\Theta}_{(t)}$,	$\frac{d\vec{\Theta}}{dt} = f(\vec{\Omega}, \vec{\Theta} \ldots)$	aircraft Euler angles, angle/rotation relations
$\vec{U}_{(t)}$,	$\frac{d\vec{U}}{dt} = f(\vec{U}, \vec{\Omega}, \vec{F} \ldots)$	aircraft velocity, force-equilibrium relations
$\vec{\Omega}_{(t)}$,	$\frac{d\vec{\Omega}}{dt} = f(\vec{M} \ldots)$	aircraft rotation rate, moment-equilibrium relations

II.B.4. Control model

This consists of an arbitrary number of control deflections superimposed at each surface beam location, and driven by any PID control laws implemented via user-supplied routines.

$\vec{\delta}_{(t)}$,	$\vec{\delta} = f(\vec{U}, \vec{\Omega}, t \ldots)$	control deflection variables, control laws

In addition, there are also joint relations between beams, which appear as internal or endpoint boundary conditions. Flapping motion is introduced into these beam joint relations.

All the above models are fully coupled, and the overall system is solved by a full Newton method. The overall state for a typical configuration has only $\mathcal{O}(1000)$ unknowns with mostly compact support, and executes in less than 1 second per time step. Hence, even complex flight simulations are quite economical.

II.C. Panel Method: *FastAero*

FastAero[13] is a boundary element method or panel method[17–19] for solving two-dimensional and three-dimensional potential flow. Potential flow panel methods have been used as an aerodynamics tool since their initial development. Their success has been largely due to the high fidelity surface geometry representation combined with their computational efficiency. Potential flow panel methods are based on the solution of Laplaces equation in integral equation form. Despite the simplifications introduced by potential flow (inviscid, irrotational flow), the methods are powerful and accurate when analyzing the aerodynamic behavior of streamline shapes. Although, it is likely that flapping wings will experience flow separation, it is likely not a desired state due to the increased energetic demands. As such, it is assumed that birds and bats, as well as engineered vehicles, during regular flight, will not have significant regions of separation.

The two-dimensional version of FastAero includes a traditional source-doublet Dirichlet formulation and a traditional doublet-only Neumann formulation. The unknowns on the airfoil and in the wake are represented using linear basis functions.[18] An iterative GMRES solver[20] is implemented to solve the resultant linear system; however, unlike the three-dimensional version of FastAero, no matrix vector product acceleration is performed. The time dependent circulation on the wing is determined using a Kutta condition which imposes a wake potential jump which invokes no infinite velocities at the trailing edge. Changes in wing circulation over time are accounted for in the trailing dipole wake. The linear strength dipole wake panels can be either held fixed in space or convected using the local velocity field. The forces and pressures on the airfoil are computed using the unsteady Bernoulli Equation. To approximately account for viscous effects in FastAero2D, a drag polar approximation is used. The drag polar approximation considers the static drag polar of the actual airfoil and penalizes drag separately (by imposing high drag coefficients on airfoils whose incidence angles are above a cetain prescribed value).

The three-dimensional version of the FastAero Panel Method is an unsteady, accelerated, panel method with convected vortex particle wakes. In this section we highlight the methodology used, and refer to the original reference[13] for a more complete description of the method. The method uses linear strength basis functions[25] to represent the distribution of source and dipole strength on each of the elements in the discretization. As in the two dimensional case, the solver is capable of representing aerodynamic flows using a source-dipole Greens Theorem formulation to solve the Dirichlet problem, while the Neumann problem can be solved using dipoles and/or sources. The method represents the wake vorticity and handles unsteady wake evolution through the use of a vortex particle method.[21–24] Computational efficiency is a fundamental consideration when simulating unsteady, morphing body, three dimensional flow due to the requirement that many solutions be determined using a time-stepping procedure. The computational efficiency of the method scales nearly linearly with the number of unknowns in the problem ($\mathcal{O}(nlog(n))$) due to the use of iterative solution methods[20] combined with matrix vector product acceleration. The precorrected-FFT[27] acceleration is considered for body-panel interactions and solutions and a fast multipole tree algorithm[26] is considered for wake-wake interactions. The 3D solutions computed with FastAero are not corrected for viscous drag effects, therefore, only induced drag quantities are considered. This lack of viscous modeling hinders the methods' ability to predict flow separation as well as provide an estimate of the total power (since the total power will have a significant viscous contribution).

II.D. Navier Stokes Solver : *3DG*

The highest fidelity level which we consider represents the full physics of the fluid. We solve the compressible Navier-Stokes equations using a Discontinuous Galerkin (DG) high order discretization technique. High order methods are advantageous for applications requiring low numerical dispersion and high time accuracy. They are also particularly well suited for problems involving multiple spatial and temporal scales. For instance, our DG algorithm is able to compute accurate solutions to the compressible Navier-Stokes equations for Mach numbers as low as $10^{-3} - 10^{-4}$. The DG method produces stable discretizations of the convective operator for any order discretization, thus avoiding the need for additional stabilization or filtering. Here,

we use nodal basis and polynomial orders in the range $p = 3 - 5$. The viscous terms are discretized using the Compact Discontinuous Galerkin (CDG) method[30] which leads to optimal accuracy, is compact and generates sparser matrices than the alternative existing methods. The CDG method has similar properties to the LDG method[33] but has the added benefit of being compact.

In order to obtain maximum geometrical flexibility the Navier-Stokes equations are discretized on unstructured meshes of triangles and tetrahedra. Due to the high level of resolution provided by the high order methods, we are able to resolve laminar flows up to $Re \sim 2-4\cdot 10^4$ using isotropic meshes. Figure 4 illustrates this point for the unsteady flow about a laminar foil at an angle of attack just above C_{Lmax}. It is noted that the laminar boundary layer can be accurately captured within 1-2 elements with $p = 4$ order polynomials. For turbulent flows, high order DG methods are able to produce grid converged solutions using considerably less degrees of freedom that the alternative lower order methods. A resolved sample solution using $p = 4$ approximations for a subsonic turbulent flow is shown in figure 5. The DG high order Navier-Stokes solver

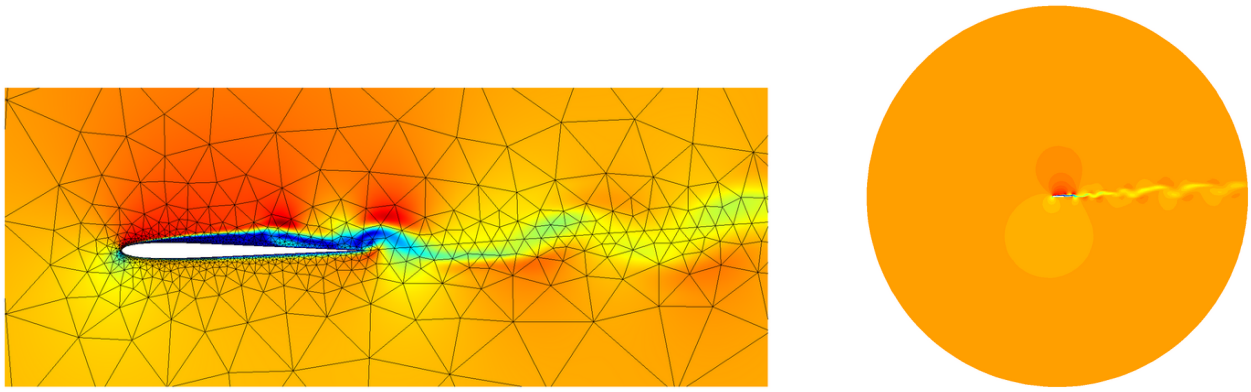

Figure 4. Unsteady flow over a laminar airfoil at $Re = 20,000$. Mach number contours. On the right we note how the wake is resolved downstream of the airfoil, even with a very coarse discretization.

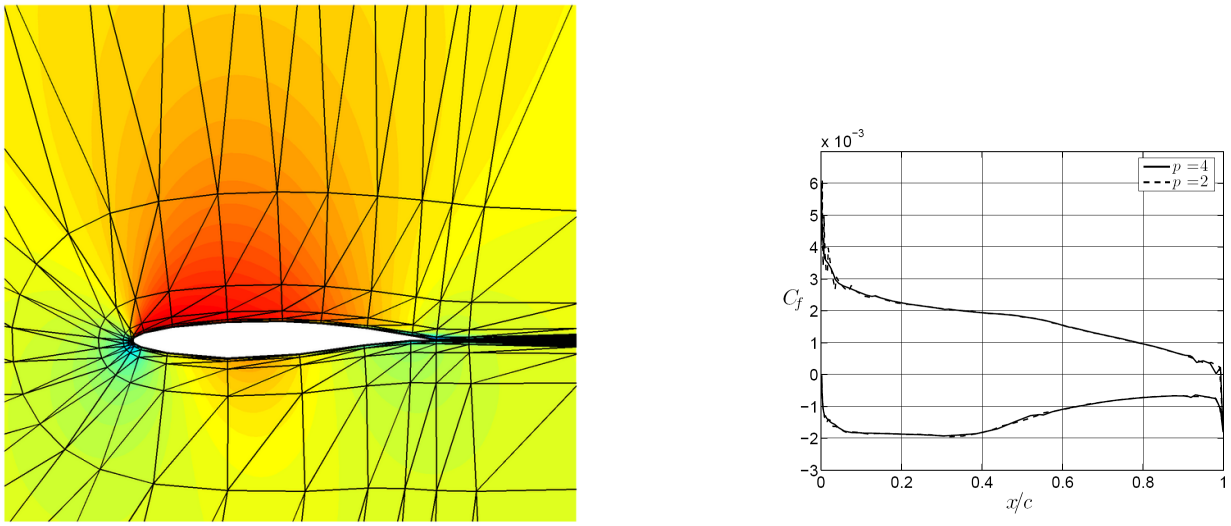

Figure 5. Turbulent flow about an RA2822 at $Re = 5 \cdot 10^6$ and $Ma = 0.1$. The Mach solution for $p = 4$ together with the discretization employed is shown on the left. On the right, the skin friction computed is compared with that obtained with a $p = 2$ solution using approximately the same number of degrees of freedom

can solve time dependent laminar and fully RANS (using the Spalart-Allmaras model) flows in 2 and 3 dimensions. The time integration can be carried out both implicitly and explicitly. For implicit integration, a Newton iteration with a Krylov solution for the resulting linear systems is used at each iteration. A robust preconditioner[31] based on a combination of ILU(0) and coarse grid correction, allows for the solution of the resulting linear system of equations using a GMRES method.[20] This preconditioner is implemented together with a dense block matrix storage model for the Jacobian matrix. For explicit time integration we employ a fourth order Runge-Kutta method.

In order to accommodate time changing geometry, the 3DG code considers an Arbitrary-Lagrangian-Eulerian (ALE) formulation for the Navier Stokes equations on deformable meshes.[32] A mapping $\boldsymbol{\psi}(\boldsymbol{\chi}, t)$ between a fixed reference domain V_χ and the physical time dependent domain $v(t)$ is introduced. The original Navier-Stokes equations written on $v(t)$ can then be transformed to an equivalent conservation law for the reference domain V_χ.

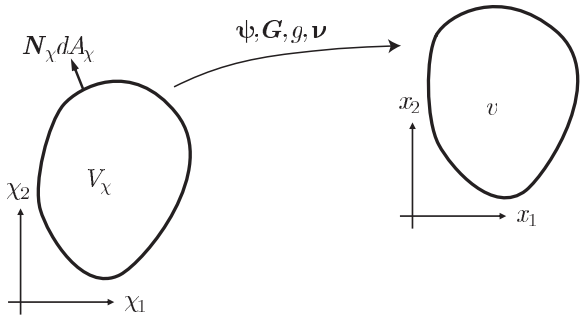

Figure 6. Reference V_χ, and current v configurations

Thus, the Navier-Stokes equations

$$\left.\frac{\partial \mathcal{U}}{\partial t}\right|_x + \boldsymbol{\nabla}_x \cdot \boldsymbol{\mathcal{F}}_x = 0$$

written in the spatial domain (x, t) for a conserved variable vector $\mathcal{U}$ with spatial fluxes $\boldsymbol{\mathcal{F}}_x$ can be written in terms of the reference independent variables (χ, t) as

$$\left.\frac{\partial \mathcal{U}_\chi}{\partial t}\right|_\chi + \boldsymbol{\nabla}_\chi \cdot \boldsymbol{\mathcal{F}}_\chi = 0 \ ,$$

where the transformed variable and flux vector are

$$\mathcal{U}_\chi = g\mathcal{U}_x \quad , \quad \boldsymbol{\mathcal{F}}_\chi = g\boldsymbol{G}^{-1}\boldsymbol{\mathcal{F}}_x - \mathcal{U}_\chi \boldsymbol{G}^{-1}\boldsymbol{\nu}.$$

These expressions involve the deformation gradient of the mapping $\boldsymbol{G} = \boldsymbol{\nabla}_\chi \boldsymbol{\psi}$ and the determinant of the deformation gradient g as well as the grid velocity $\boldsymbol{\nu} = \left.\frac{\partial \boldsymbol{\psi}}{\partial t}\right|_\chi$.

When discretizing these modified equations in the fixed reference domain (χ, t), special care must be taken to ensure satisfaction of the Geometric Conservation Law (GCL).[28,29] In our case, the satisfaction of the geometric conservation law is obtained by simultaneously integrating an equation for the determinant of the mapping g. This allows us to correct for numerical errors incurred during the time integration and thus exactly preserve the free stream conditions.[32] We note that when the mapping $\boldsymbol{\psi}(\boldsymbol{\chi}, t)$ consists of a rigid body motion, i.e. translation and/or rotation, then $g = 1$ and in this case no additional equation needs to be solved to preserve the geometric conservation law.

III. Applications of the Computational Framework

In order to demonstrate some of the uses of the computational framework we present the following representative examples:

- **Passive structures for thrust generation in two-dimensions**: Although conceptually a simple problem, the goal of this example is to illustrate the use of the tools in a design oriented problem. The analysis illustrates the insight and results which can be achieved using a multi-fidelity approach.
- **Inverse design of three dimensional flapping wing shapes**: This example illustrates some of the capabilities of the framework in three dimensions. The goal here is to determine the flapping motions and wing shape for an efficient, lift and thrust producing wing. The example further illustrates the possibility of using wake only methods to commence the design and development process for efficient flapping vehicle concepts.

- **Simulation of a Bird-Like Geometry**: In this example, the first steps in analyzing a realistic bio-inspired geometry are illustrated. Using ASWING a falcon like geometry is simulated illustrating articulated wings and balance of flight forces.

III.A. Example 1: Efficient, Passive 2-Dimensional Thrust Generation

In this conceptually simple example, the design of an efficient, thrust producing, harmonically driven flapping foil is considered. Although two-dimensional flapping foils have been analysed using many different computational and experimental approaches,[8,16] we present a design driven, multi-fidelity investigation for examining the problem. The configuration of interest is illustrated in figure 7. In this example a heaving

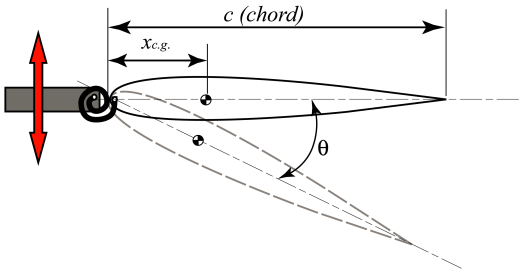

Figure 7. An illustration of the airfoil geometry used in this investigation. The unknown spring coefficient C_{spring} is determined along with flapping parameters (such as flapping amplitude and flapping frequency) such that the thrust production is performed with high efficiency.

motion is prescribed such that the vertical position $h(t)$ of the airfoil is defined by:

$$h(t) = \cos(\omega t). \tag{3}$$

In addition to the heaving motions, the airfoil is assumed to heave in a flow with velocity, $U = [1, 0, 0]$. Given this simple harmonic heaving motion, the goal is to determine the heaving amplitude A, the frequency ω, and the leading edge spring constant C_{spring}, which maximizes thrust production efficiency. Even in the case of this simple problem, it is clear that there are several parameters which must be tuned. The multi-fidelity framework is applied to this example using the following steps:

1. The wake only HallOpt method is used to determine the optimal frequency and amplitude of flapping.
2. The wake only analysis combined with a basic structural inverse design is used to determine an initial guess for the spring constant.
3. The flapping Strouhal number range and spring constant range determined in the previous step is used to guide a design space sweep using the 2D FastAero solver.
4. Finally, a series of high fidelity Navier Stokes solutions is performed and compared with the low and medium fidelity solvers.

In the sections which follow, a more detailed description of the various steps in the process is presented.

III.A.1. Wake only analysis: Frequency and Amplitude for Minimum Power at a Specified Thrust

The wake only HallOpt method is used to perform a nested optimization investigation of two-dimensional flapping (similar to Hall et al.[9]). To do this, a solution for the minimum power coefficient is computed for each combination of amplitude and frequency in the design space range. This sweep over different amplitudes and frequencies is done once per desired thrust constraint. Since the HallOpt method solves the problem rapidly, this design space sweep can be performed in a fraction of the time it takes to run a single high fidelity analysis. The results of the design space sweep are presented in figure 11. The results illustrate that the most efficient flapping configuration for thrust production ($C_T = 0.1 - 0.4$) has a $St = [0.2, 0.5]$. In addition, from this design space sweep, it can also be observed that the flapping Strouhal number should increase with increased thrust requirement.

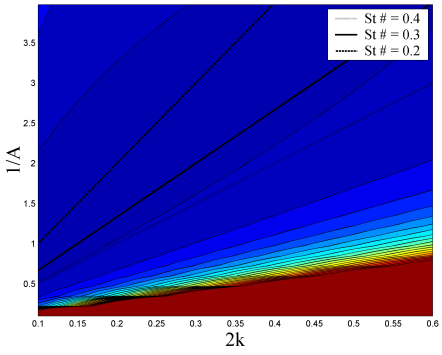

(a) $C_{T_1} = 0.1$

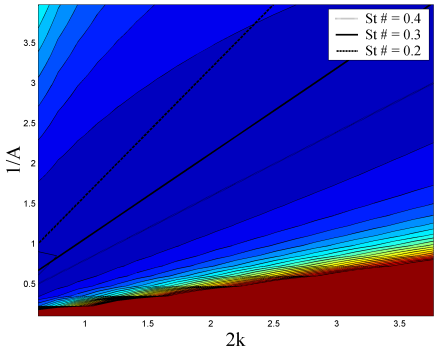

(b) $C_{T_1} = 0.2$

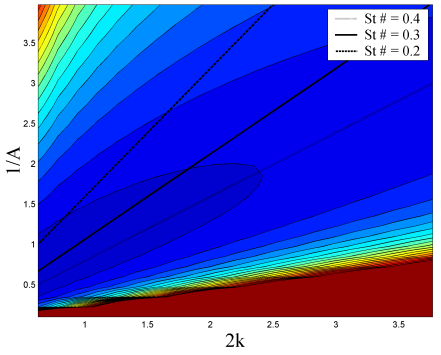

(c) $C_{T_1} = 0.3$

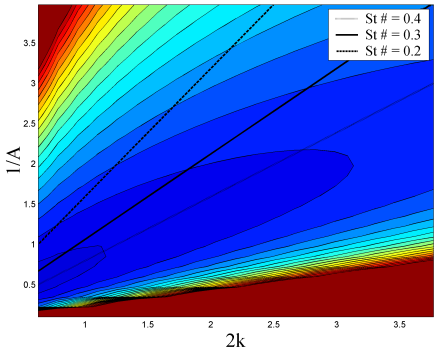

(d) $C_{T_1} = 0.4$

Figure 8. An illustration of the coefficient of thrust (C_T) as a function of the amplitude (A) and the flapping frequency ($2k = \omega$). Note in this example that the ordinate is the inverse of the amplitude, to facilitate the portrayal of the Strouhal Number. In addition to the coefficient of power, the figure also illustrates several lines of constant Strouhal Number. As can be seen, the majority of efficient flight occurs in the Strouhal Number range of $[0.2, 0.5]$.

III.A.2. Wake only analysis: Spring Constant Predictions for Minimum Power at a Specified Thrust

Following the initial investigation of the frequency and amplitude dependence of efficient flapping motions, an investigation of the passive structural strategy is undertaken. As shown in figure 9a, a phase shift of nearly $\frac{\pi}{2}$-radians exists between the circulation distribution and the wake trace. To achieve this, the airfoil must undergo pitching motions out of phase by $\approx \frac{\pi}{2}$-radians from the driving heaving motions. A simple approach to passively achieve this phase shift is to introduce a leading edge torsional spring into the heaving/plunging system.

In order to predict the structural compliance(spring constant), a massless airfoil shape (HT-13) and size(chord = 1) is selected. The following moment equation is satisfied at the leading edge of the wing (note: the design problem becomes more complex with an airfoil with mass, but the underlying process would be conceptually similar):

$$M_{L.E.} = M_{aero} + C_{spring}\theta = 0 \tag{4}$$

To compute the aerodynamic moment about the leading edge of the airfoil as well as to determine the angle of incidence of the airfoil, the circulation distribution required to produce the necessary thrust is used:

$$M_{aero} = \rho U_i \Gamma x_{\frac{c}{4}}. \tag{5}$$

The incidence angle of the airfoil to the local relative flow is determined using:

$$\alpha = \frac{\Gamma}{\pi U_i c} \tag{6}$$

Finally, the overall angle θ of the airfoil in the flow is computed as:

$$\theta(t) = \tan^{-1}\left(\frac{U_{yi}(t)}{U_{xi}(t)}\right) - \alpha(t) - \alpha_i(t) \tag{7}$$

where, $\alpha_i(t)$ is induced effect of the wake-induced velocity on the airfoil. With a known circulation distribution Γ and a prescribed heaving motion, the only unknown in equation 4 is the spring constant (C_{spring}). Since the optimal spring constant varies throughout the flapping cycle, a leading-edge-moment, weighted least squares solution is applied to determine a single, near optimal spring constant. This computation can be efficiently performed over a range of parameters. The resulting design space sweep involves computing the power coefficient and spring constant for each of the thrust coefficients and Strouhal numbers of interest. These results are illustrated in figure 9, showing that in the region of optimal thrust production the leading edge spring constant ($C_{spring} \approx 0.1 - 0.25$) does not vary significantly.

The HallOpt wake only method in this example provided some simple approaches for examining the large design space. By performing several rapid design space sweeps, the medium and high fidelity tools can be invoked to more closely examine the region of interest.

III.A.3. Panel Method Design Space Sweep:

Using the spring constant and flapping Strouhal number results from the parameter sweeps as a guide, a potential flow design space sweep is performed. For this particular design space investigation, a symmetric HT-13 airfoil is selected as the geometry due to its positive properties at low Reynolds numbers. Figure 7 illustrates the geometry under consideration. The following design space parameter ranges were considered for a flapping reduced frequency of $\omega_r = 0.1$, and $\omega_r = 0.4$:

$$C_{spring} = [0.05, 0.5] \tag{8}$$

$$St = [0.05, 0.55] \tag{9}$$

The results of these design space sweeps are presented in figure 12. For this simulation the efficiency is computed as:

$$\eta_{prop} = \frac{P_{OUT}}{P_{IN}} = \frac{\int F_x V_x dt}{\int \vec{F}_y V_y dt} \tag{10}$$

The leading edge moment is not included in the efficiency computation, since the spring at the leading edge is assumed to be perfectly lossless. The results of the design space sweep using the predicted spring

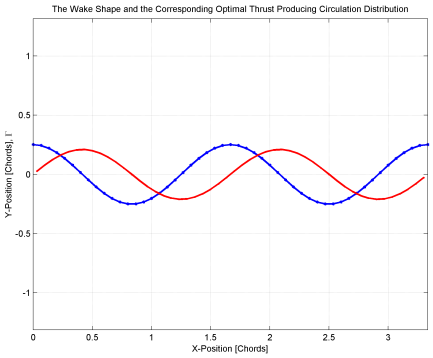

(a) A plot of the optimal wake circulation (red) and the wake trace (blue). Note that the time-varying wake circulation and the wake path are $\approx \frac{\pi}{2}$ out of phase.

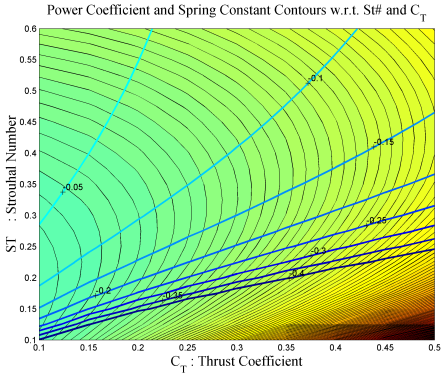

(b) High Reduced Frequency

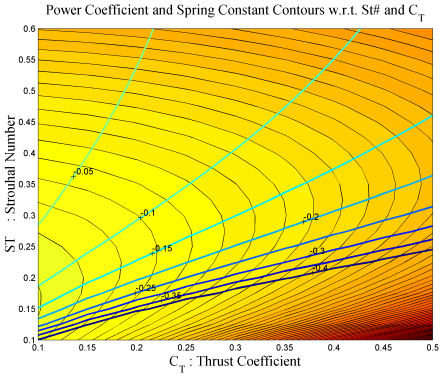

(c) Moderate Reduced Frequency

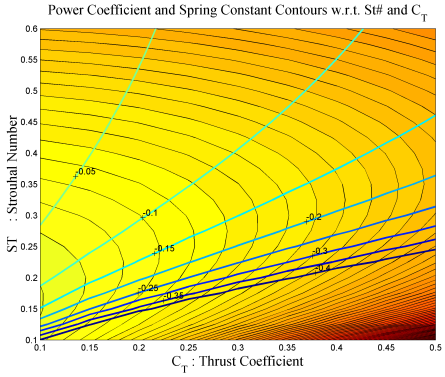

(d) Low Reduced Frequency

Figure 9. Plot (a) illustrates the circulation distribution required for optimal thrust production for the particular heaving motion selected. Figures (b)-(d) illustrate the HallOpt prediction of the spring constant. In the figures, the filled contours represent the power required to produce the required thrust, while the line contours represent constant spring stiffness. As can be observed from the figure, the optimal thrust production can be achieved with relatively small deviations in the spring constant.

constant and Strouhal number range indicate good agreement with the wake only design space predictions. Furthermore, from the plots (see figure 12), it can be see that there is a large region of high efficiency near the optimal design point, thus, it is likely that an appropriately chosen single torsional spring could be used to achieve many different thust configurations.

III.A.4. High Fidelity Design Space Sweep

The high fidelity design sweep involves using 3DG to perform design space sweep simulations. The fluid properties in the simulation are $\mathrm{Re} = 5 \cdot 10^3$ and $\mathrm{Ma} = 0.2$. The leading edge of the airfoil is prescribed using the same sinusoidal motion as in the medium fidelity case (vertical motion set by a reduced frequency and amplitude) yielding a specific Strouhal number. The spring is given a natural frequency (determining the spring constant C_{spring}) that alters the airfoil's propensity to conform to the fluid motion. The moment equation is solved simultaneously with the flow equations in order to capture the fluid-structure (spring) interaction. The particular moment equation being solved at the leading edge of the airfoil is:

$$I\ddot{\theta} + C_{spring}\theta + S\ddot{h} - M_{aero} = 0 \tag{11}$$

where, $S = m_{airfoil}x_{cg}$ is the static unbalance.

The simulations are performed as close to massless as possible setting moment of inertia $I = 0.033$ and mass moment about the pivot $S \approx I/0.3 = 0.1$.

The simulation commences with the airfoil configured at the top point of the amplitude in the spring's vertical motion and at zero angle of attack (initializing the most steady configuration to begin the pitching and heaving motion of the airfoil within the flow). As with the medium-fidelity solver, 3DG was run for two design sweeps of St number and C_{spring} involving two reduced frequencies, giving a 4×5 sweep for $\omega_r = 0.1$ and 6×6 sweep for $\omega_r = 0.4$, where

$$St = [0.05, 0.51] \tag{12}$$

$$C_{spring} = [0.05, 0.75] \tag{13}$$

The simulations were run until the force generation stabilized which occurred at 3-4 periods of pitching and heaving. Both the propulsive efficiency and coefficient of thrust are computed and shown in Figure 12 and 13. The results are similar to the predictions of the lower fidelity methods, yielding efficient flight for softer spring driven ($C_{spring} = 0.1 - 0.3$) heaving at $St = 0.1 - 0.4$ for a specific thrust requirement. Despite slightly advantageous thrust generation for a higher spring constant parameter, as the C_{spring} increases the likelihood of stall also increases. When the airfoil stalls, there is a reduction in efficiency. Analyzing the data requires averaging thrust or efficiency computed from various period iterations after the flow force/power generation stabilizes; however, for the cases where stall occurs the thrust generation continues to be unsteady regardless of simulation time. However, the separated flow is correctly modeled in this higher fidelity model and thus, predicts this flow regime the most accurately within this multi-fidelity framework (see figures 13-14). In conclusion, 3DG design sweeps adds richness to the region of optimality predicted by the lower fidelity simulations and computations and also enhances the results for this efficient, passive two-dimensional thrust generation model in the separated flow regime. It can be seen that high fidelity methods are valuable tools for confirming predictions from lower fidelity level predictions. Finally, to end this example the time evolution of forces as predicted by the high fidelity solver and panel method are compared in figure 13.

III.A.5. Conclusions: Two-Dimensional Design Space Sweep

The two-dimensional heaving airfoil design space sweep which is performed, illustrates the multi-fidelity framework applied to a model problem in the flapping propulsion realm. Although this experiment does not draw formal conclusions about thrust generation and passive structural design in nature, it does exhibit that the computational framework which has been assembled is consistent and successful at finding the optimal region of the design space.

III.B. Example 2: Designing Efficient Flapping Wings in 3-Dimensions

Due to the initial success of the multi-fidelity framework in two-dimensions, some effort has been applied to developing a similar design pathway in three-dimensions. The goal in three-dimensions is to develop

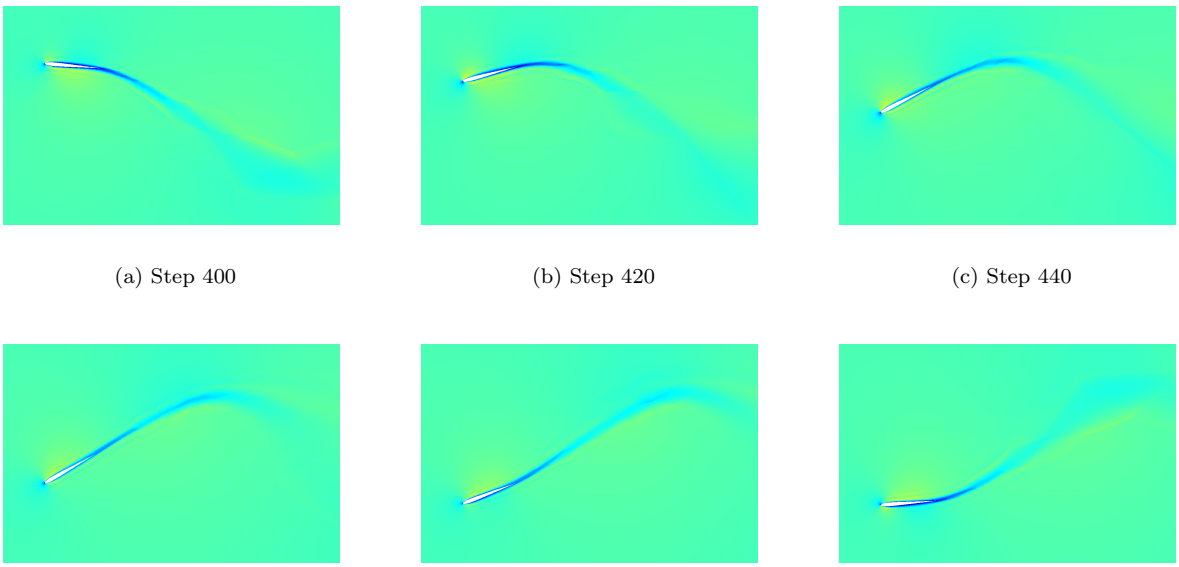

(a) Step 400 (b) Step 420 (c) Step 440

(d) Step 460 (e) Step 480 (f) Step 499

Figure 10. Several snapshots of the high fidelity solution for a spring constant $C_{spring} = 0.056$, $\omega_r = 0.4$, and $St = 0.24$. In these images, the color scale indicates the Mach number. In this case the spring constant is small, and the flow remains attached throughout the flapping cycle.

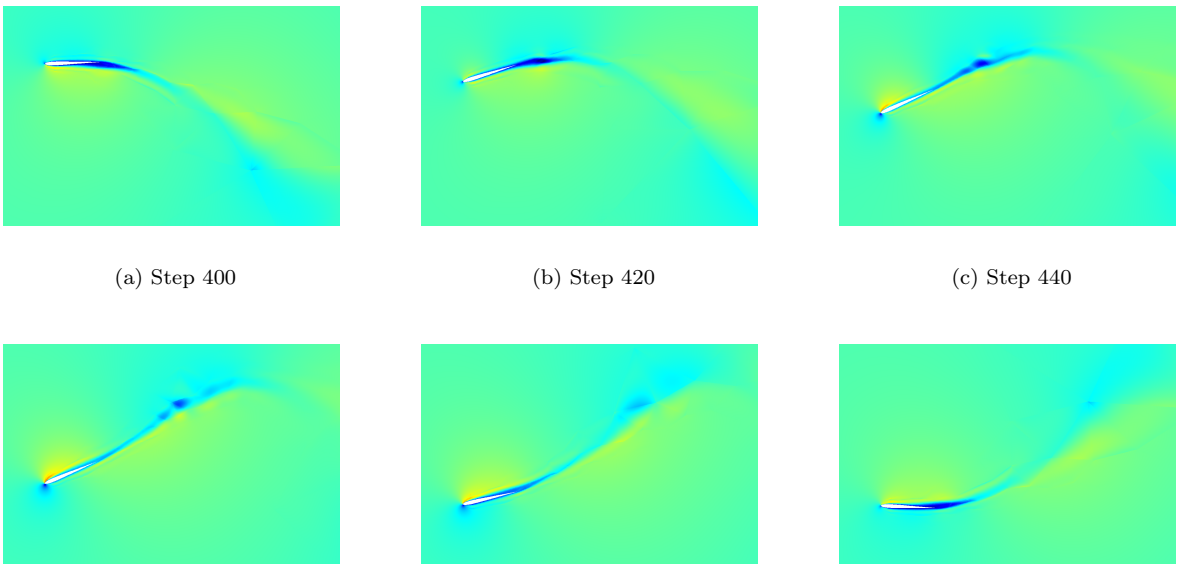

(a) Step 400 (b) Step 420 (c) Step 440

(d) Step 460 (e) Step 480 (f) Step 499

Figure 11. Several snapshots of the high fidelity solution for a spring constant $C_{spring} = 0.363$, $\omega_r = 0.4$, and $St = 0.24$. In these images, the color scale indicates the Mach number. Notice the considerable flow separation during heaving, which would not be modeled accurately using lower fidelity models

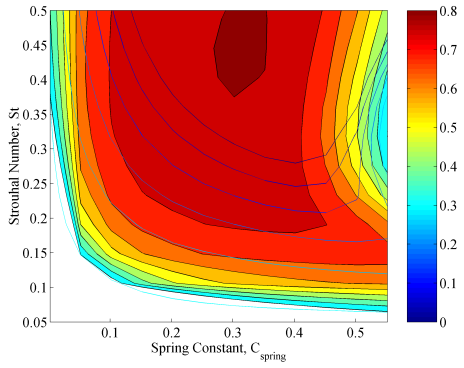

(a) FastAero2D Design Space Sweep Simulations, $\omega_r = 0.1$

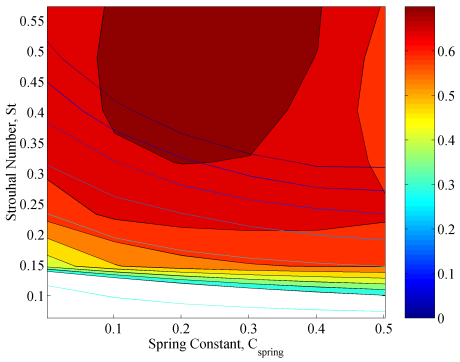

(b) FastAero2D Design Space Sweep Simulations, $\omega_r = 0.4$

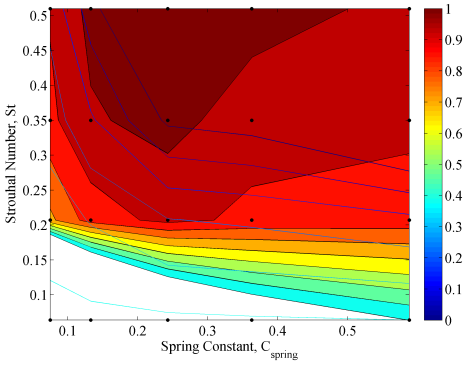

(c) 3DG Design Space Sweep Simulations, $\omega_r = 0.1$

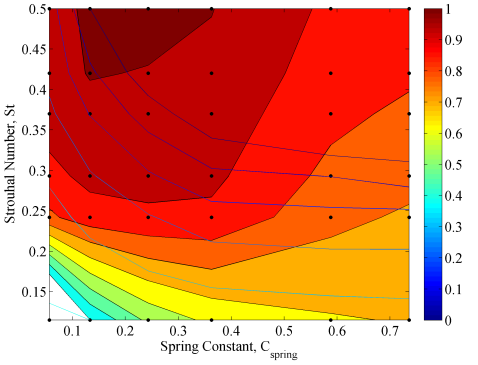

(d) 3DG Design Space Sweep Simulations, $\omega_r = 0.4$

Figure 12. A comparison of the FastAero design space simulation with the 3DG simulation in a similar region of the design space. Notice, that due to the desire to use the design tools most appropriately that the design spaces covered are not exactly identical. The filled contours represent the efficiency of the thrust production (including viscous effects) while the lines indicate lines of constant thrust. In order to gain the most efficient flapping strategy for a given spring constant the aim is to find the region along a line of constant thrust at which the flight efficiency is maximized. As can be seem this maximum efficiency point for the different predictions starts out with a low Strouhal number and low spring constant for lower thrust requirements, while higher thrust requirements must be met with more vigorous flapping, and higher spring constants.

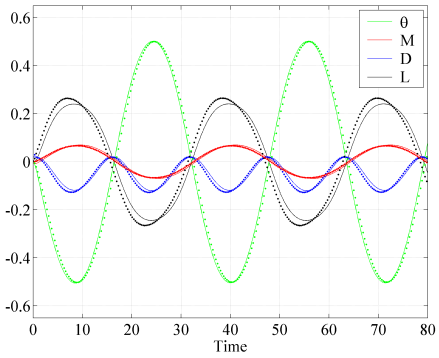

(a) Time Evolution of Forces for $C_{spring} = 0.133$, $St = 0.207$ and $\omega_r = 0.1$, FastAero2D vs. 3DG

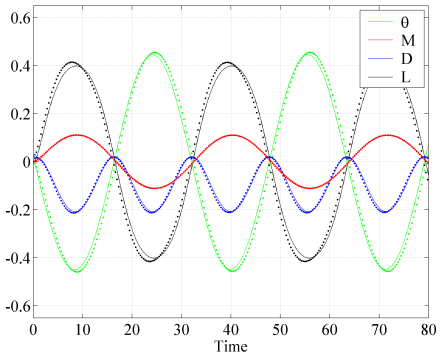

(b) Time Evolution of Forces for $C_{spring} = 0.243$, $St = 0.207$ and $\omega_r = 0.1$, FastAero2D vs. 3DG

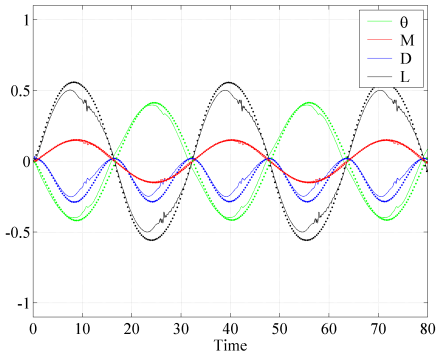

(c) Time Evolution of Forces for $C_{spring} = 0.363$, $St = 0.207$ and $\omega_r = 0.1$, FastAero2D vs. 3DG

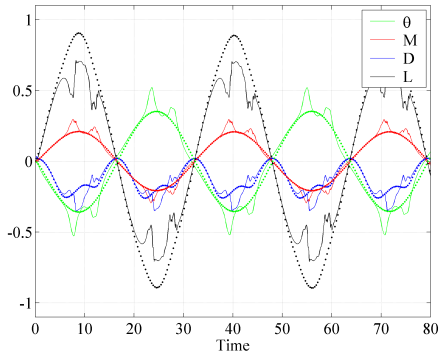

(d) Time Evolution of Forces for $C_{spring} = 0.588$, $St = 0.207$ and $\omega_r = 0.1$, FastAero2D vs. 3DG

Figure 13. A comparison of the FastAero2D (discrete dots) and 3DG (solid lines) time evolution of forces for several characteristic parameters during the heaving of the airfoil. For these comparisons, the reduced frequency is low ($\omega_r = 0.1$). Notice that the difference between the methods is significant when the flow separates. In these cases, a high fidelity solver such as 3DG, must be used for accurate predictions of the thrust production behavior.

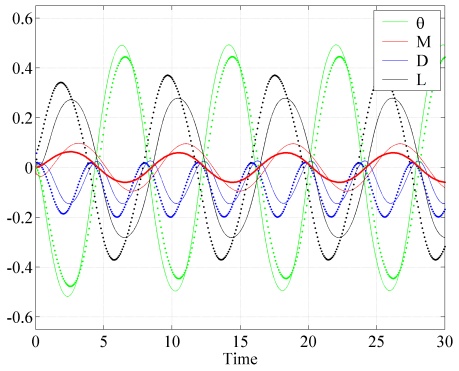

(a) Time Evolution of Forces for $C_{spring} = 0.133$, $St = 0.24$ and $\omega_r = 0.4$, FastAero2D vs. 3DG

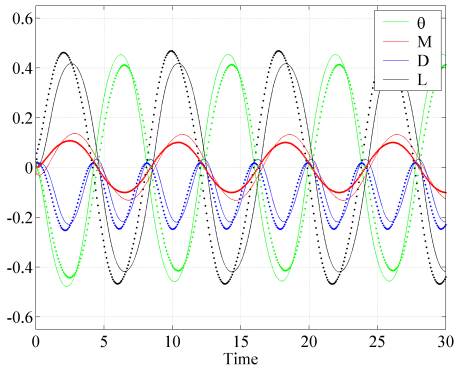

(b) Time Evolution of Forces for $C_{spring} = 0.243$, $St = 0.24$ and $\omega_r = 0.4$, FastAero2D vs. 3DG

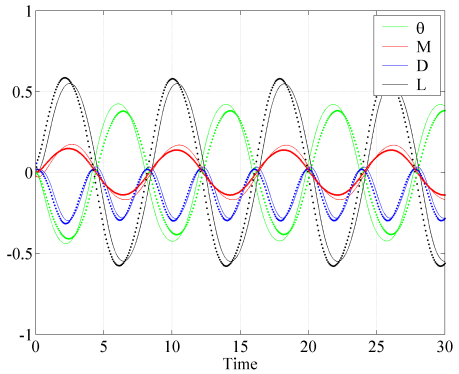

(c) Time Evolution of Forces for $C_{spring} = 0.363$, $St = 0.24$ and $\omega_r = 0.4$, FastAero2D vs. 3DG

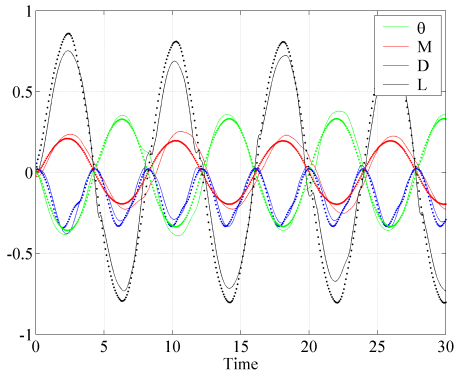

(d) Time Evolution of Forces for $C_{spring} = 0.588$, $St = 0.24$ and $\omega_r = 0.4$, FastAero2D vs. 3DG

Figure 14. A comparison of the FastAero2D (discrete dots) and 3DG (solid lines) time evolution of forces for several characteristic parameters. The airfoil is plunged at a more aggressive reduced frequency ($\omega_r = 0.4$). The simple finite velocity Kutta condition is likely responsible for some of the reduction in accuracy of the panel method at this reduced frequency. In these simulations, discrepancy between the two methods is also displayed at lower spring constants, where the angular orientation of the airfoil is likely to be heavily dictated by visous effects (visous feathering), and hence, a deviation between the two predictions starts to occur.

a strategy for designing flapping wings which are as structurally passive as possible. Prior to considering structural compliance, the shape to which the wing must deform during flapping must be determined. In this section we illustrate a simplistic strategy for accomplishing this inverse shape design in a 3-Dimensional setting. In this example the washout of the wing is adjusted to produce the desired circulation in the wake (whereas, more complicated arrangements might consider both washout and local section cambering). In order to design a flapping wing based on the HallOpt optimal wake the following steps are performed:

1. The plan-form of the wing is determined. This includes the chord dependence on the spanwise position. Since the HallOpt viscous correction relies on the chord, it is important that the wing introduced into the solution has the correct plan-form.

2. Given the planform, a feathered flapping wing shape must be determined. This step involves determining the shape of the flapping wing, that when driven to flap, has the least amount of force production. This is currently a two-step process. First the wing sections are aligned with the local flow. For high aspect ratio wings undergoing relatively simple flapping motions, the forces on the wing are low after initial alignment with the flow. The second step in the wing-feathering process is to simulate and correct the initial guess of the feathered state. This step involves simulating the flow aligned wing in FastAero, and then postprocessing the result to minimize the circulation in the wake.

3. Once a feathered wing is obtained, the following steps are repeated until a level of convergence is achieved:

   - Determine the wake shape which results from the trace of the trailing edge of the feathered/deformed wing.
   - Determine the optimal wake circulation distribution in that trace by solving the wake only HallOpt problem.
   - Compute the downwash at each of the chordwise sections at each step in the wake.
   - Determine the additional incidence required for the wing to produce the desired wake circulation distribution (prescribed by the HallOpt method)
   - Update the deformed wing shape and iterate. These iterations are currently simple weak iterations, and are normally stopped after 3-5 steps.

4. Once the deformed wake shape and wing shape have converged, the discretized surface geometry of the wing can be constructed. Given the geometry, the wing can be analysed using any of the geometry based solution methodologies.

To illustrate this three-dimensional flapping wing design process a straight leading edge wing, with span = 1 and a chordwise distribution:

$$c(y,z) = \frac{1}{8} - \frac{1}{2.25}\left(P_y^2 + P_z^2\right), \tag{14}$$

can be used. The flapping reduced frequency was selected to be ≈ 0.25. The wing-beat flapping angles were chosen to be ± 25 degrees. An illustration of the feathered wing, and first iteration of the loaded wing is presented in figure 16. The geometry presented above was simulated using the FastAero three-dimensional panel method. An illustration of the geometry and the trailing wake is presented along with the flight forces in figure 17. In order to verify the design process for this example, the wake history from FastAero is compared with the target HallOpt wake distribution. In figure 18 the HallOpt and FastAero wakes are shown. As can be observed from that image, the two wakes are qualitatively very similar.

III.B.1. Conclusions: The inverse design of three dimensional wings

In this example it has been illustrated that the design framework can be exploited in three-dimensions. The design framework is capable of providing an initial wing design for simulating in higher geometric fidelity computational tools. The success of this simple wing design problem illustrates the potential benefits of using a diverse array of multifidelity methods for flapping wing analysis and design.

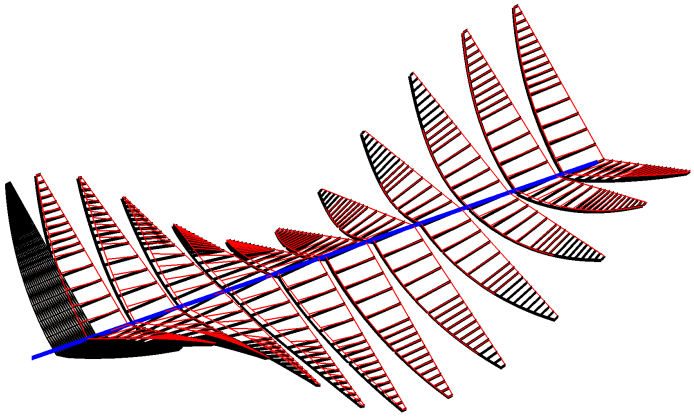

Figure 15. The feathered wing (red) is illustrated in side view projection with the final loaded wing design (black). It is clear in this image that the morphability of this wing is primarily exploited in determining the feathered wing shape, and that the loaded wing shape is a perturbation on top of that.

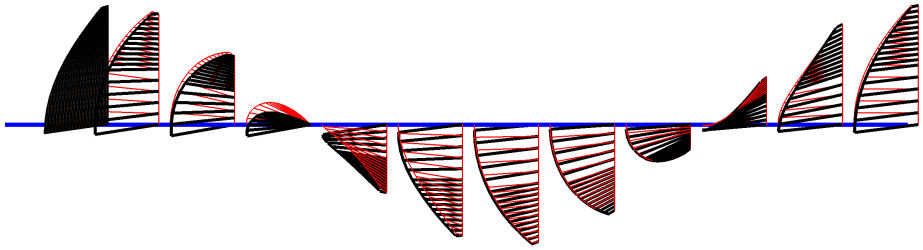

Figure 16. The initial feathered wing (red) is illustrated in conjunction with the final loaded wing design (black). Snapshots are shown in a three-dimensional projection.

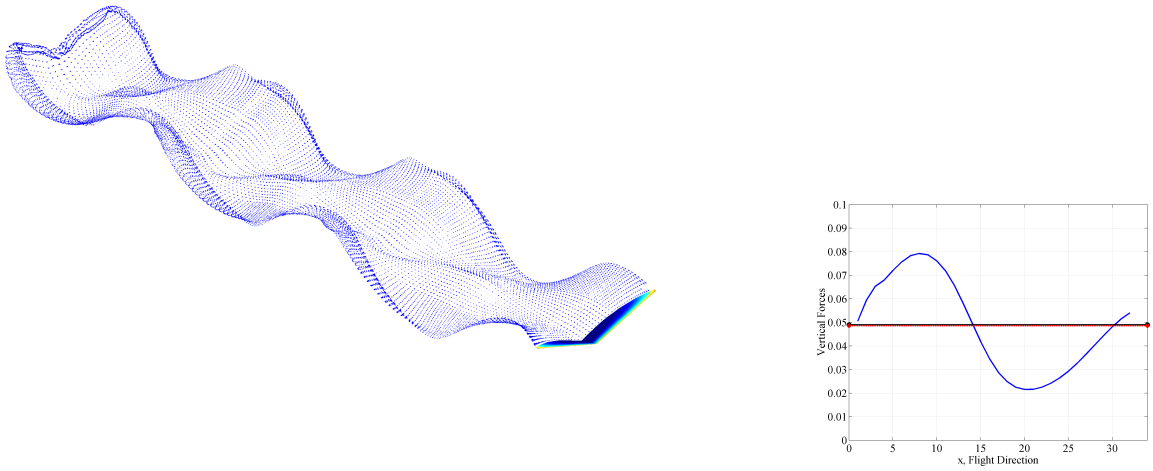

Figure 17. (left) A plot showing the wing and wake geometry for an inverse designed wing shape. In the image, the vortex rollup during wing downstroke is clearly observed. (right) The corresponding time dependent lift forces (blue) and time averaged forces (red dashed line) are presented. In addition, the target design time-averaged lift forces from the HallOpt problem are shown(black). The results illustrate good agreement for the lift average force over a period. A different strategy involving both camber and wing angle of incidence variations would likely be a more realistic arrangement for efficient lift and thrust production.

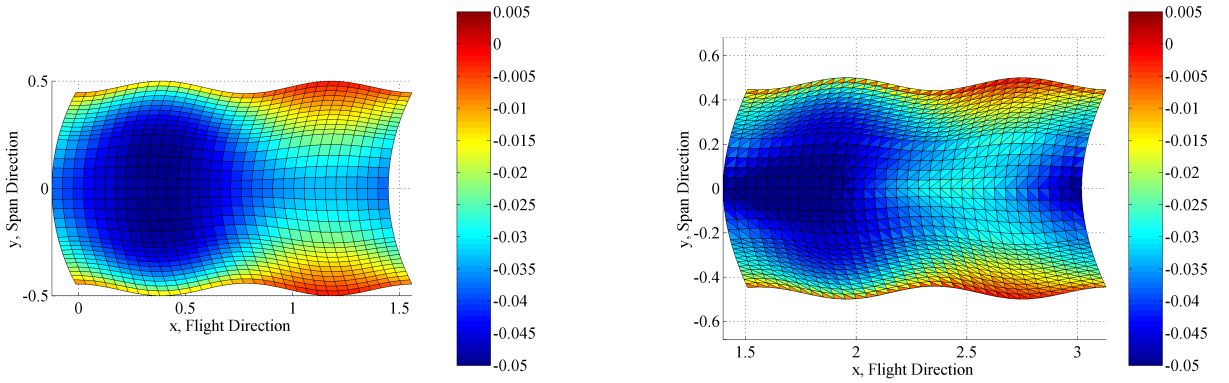

Figure 18. (left) The desired wake circulation distribution for the current configuration is computed using HallOpt. (right) The final wake circulation distribution (computed using FastAero) in the wake after the approximate inverse shape design is performed. The final wake circulation distribution is determined from a FastAero simulation of the morphing wing geometry. The FastAero wake prediction is the second period of the wake. Apart from some minor mismatch in the circulation distribution near the midline of the wing, the wakes compare well. One possible reason for the mismatch along the wing centerline is the sharp intersection which exists between the left and right wing (which is not accounted for in this simple inverse design).

III.C. Example 3: Simulating Bird-like geometries in ASWING

In this example we illustrate simulation of flapping geometries in ASWING. The approach for handling flapping geometries in ASWING involves prescribing the joint angles and their rates of change. The simulation examined in this example illustrates the coupling of the aerodynamics, structural dynamics and controls in a single flapping wing design. The case was defined using the following parameters:

Table 1. The wing flapping parameter values for the ASWING falcon example

Parameter	Value
Flapping Frequency	3.0 Hz
Inner Wing Flapping Angle Range	[+0.0, +15.0]
Outer Wing Flapping Angle Range	[-5.0 +30.0]
Lag (Inboard/Outboard)	$\frac{\pi}{2}$
Forward-Aft Flapping	[0.0, 0.0]

Figure 19 show representative snapshots of the virtual-falcon in flight.

III.C.1. Conclusions: Simulating Quasi-Realistic Flapping Vehicles

This example has shown the potential for future application of this multifidelity framework to analysing three dimensional flapping vechiles with full fluid-structure coupling and control. Using methods like ASWING can provide a good intial guess to more expensive computational tools such as FastAero and 3DG.

IV. Conclusions

In this paper a multi-fidelity computational framework capable of analyzing and designing flapping wing vehicles has been described. Through careful application of different fidelity level tools, it is possible to span the design space effectively. Although there is no replacement for the accuracy of high fidelity Navier Stokes simulations, low fidelity tools can be applied to gain insight into the parametric dependencies and provide a good initial guess for higher fidelity solvers. Not only does the proposed methodology present an opportunity for computational savings, it also provides the ability to understand the flapping flight design space.

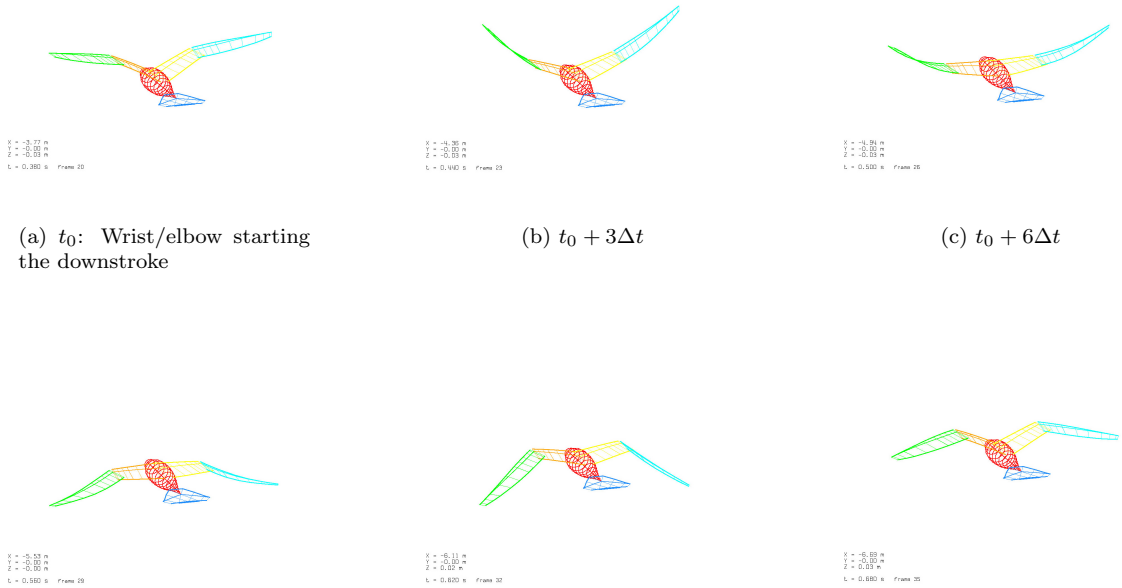

(a) t_0: Wrist/elbow starting the downstroke

(b) $t_0 + 3\Delta t$

(c) $t_0 + 6\Delta t$

(d) $t_0 + 9\Delta t$

(e) $t_0 + 12\Delta t$

(f) $t_0 + 15\Delta t$

Figure 19. Several snapshots of the ASWING simulation of a prescribed joint angle, falcon-like bird.

Acknowledgments

This material is based upon work supported by the National Science Foundation under Grant No. 0540266, Grant No. 0540203, an NSF Fellowship, and the Department of Aeronautics and Astronautics, MIT. In addition we would like to thank the Singapore-MIT Alliance for their support of this work.

References

[1]F.B.Gill,*Ornithology* W.H.Freeman and Company, New York, 2003.

[2]N.S.Proctor and P.J.Lynch,*Manual of Ornithology*, Yale University Press, New Haven, 1993.

[3]S. Swartz, *Skin and bones: the mechanical properties of bat wing tissues.* In Bats: Phylogeny, Morphology, Echolocation, and Conservation Biology, pages 109-126. Smithsonian Inst. Press, 1998.

[4]G. Neuweiler,*The biology of bats,*Oxford University Press, New York, 2001.

[5], Jones, K.D. and Center, K.B.,*Numerical Wake Visualization for Airfoils Undergoing Forced and Aeroelastic Motions,* AIAA Paper No. 96-0055, 34th AIAA Aerospace Sciences Meeting, Reno, Nevada, Jan. 1996.

[6]D. Viieru, J. Tang and Y. Lian H. Liu W. Shyy,*Flapping and Flexible Wing Aerodynamics of Low Reynolds Number Flight Vehicles*, AIAA-2006-503, 44th AIAA Aerospace Sciences Meeting and Exhibit, Reno, Nevada, Jan. 9-12, 2006

[7]Z.J. Wang,*Vortex Shedding and frequency selection in flapping flight*, Journal of Fluid Mechanics, vol. 410 pages 323-341, 2000.

[8]J Toomey and J. D. Eldredge,*Numerical and Experimental Investigation of the role of flexibility in flapping wing flight*, AIAA 2006-3211, 36th AIAA Fluid Dynamics Conference and Exhibit, San Francisco, 2006.

[9]Hall, K. C., and Hall, S. R., *Minimum induced power requirements for flapping flight* Journal of Fluid Mechanics, 1996, Vol. 323, pp. 285-315.

[10]Hall, K. C., Pigott, S. A., and Hall, S. R.,*Power Requirements for Large-Amplitude Flapping Flight* Journal of Aircraft, Vol. 35, No. 3, 1998, pp. 352-361.

[11]Hall, K. C., and Pigott, S. A., *Power Requirements for Large-Amplitude Flapping Flight,* AIAA Paper 97-0827, Presented at the 35th Aerospace Sciences Meeting and Exhibit, Reno, NV, Jan. 6-9, 1997.

[12]Graham K. Taylor Robert L. Nudds and Adrian L. R. Thomas,*Flying and swimming animals cruise at a Strouhal number tuned for high power efficiency*, Nature 425, 707-711, 2003.

[13]D.J.Willis, J.Peraire and J.K.White, *A Combined pFFT-multipole tree code, unsteady panel method with vortex particle wakes*, Int. J. Numer. Meth. Fluids, 53, 1399-1422, 2007.

[14]M. Drela,*Integrated Model for Preliminary Aerodynamic, Structural, and Control-Law Design of Aircraft*, AIAA 99-1394, AIAA 40th Structures, Dynamics, and Materials Conference, April 1999.

[15]H. Ashley, M. Landahl ,*Aerodynamics of wings and bodies*, Dover Publications, New York, 1985.

[16]Hover FS, Haugsdal O, Triantafyllou MS,*Effect of angle of attack profiles in flapping foil propulsion* J Fluid Struct, 19 (1): 37-47, Jan. 2004

[17]J.L. Hess,,*The problem of three dimensional flow and its solution by means of surface singularity distribution* Comput. Meth. Appl. Mech. Eng., 4: 283-319, 1974.

[18]J. Katz and A. Plotkin ,*Low Speed Aerodynamics*, Cambridge University Press, Cambridge, 2001.

[19]L. Morino and C.C.Luo,*Subsonic potential aerodynamics for complex configurations. A general theory.* AIAA J. 12:191-197.

[20]Y. Saad, and M. Schultz,*GMRES: A generalized Minimal Residual Algorithm for Solving Non-Symmetric Linear Systems*, SIAM, J. Sci. Comp., Vol 7, 1986.

[21]A. Leonard ,*Computing three-dimensional incompressible flows with vortex elements* , Ann. Rev. Fluid Mech., 17: 523-559, 1985.

[22]A. Gharakhani, A.F. Ghoniem,*Three-dimensional vortex simulation of time dependent incompressible internal viscous flows*, J. Comp. Phys., 134: 75-95. 1997.

[23]C. Rehbach,*Calcul Numerique d'ecoulement tridimensionels instationaires avec nappes tourbillionaires* La Recherche Aerospatiale, pp, 289-298, 1977.

[24]S.G. Voutsinas, M.A.Belessis, and K.G. Rados,*Investigation of the yawed operation of wind turbines by means of a vortex particle method* AGARD-CP-552 FDP Symposium on Aerodynamics and Aeroacoustics of rotorcraft, Berlin, Germany, Paper 11, 1995.

[25]J.N. Newman ,*Distribution of cources and Normal Dipoles Over a Quadrilateral Panel*, J. Eng. Math., 20, 1985.

[26]L. Greegard and V. Rohklin ,*A Fast Algorithm for particle simulations* , J. comp. Phys., 73: pp 325-384, 1987.

[27]J.R. Philips and J.K.White ,*A precorrected-FFT Method for Electrostatic Analysis of Complicated 3D structures* , IEEE Transactions on Computer Aided Design of Integrated Curcuits and Systems, IEEE, Vol. 16, 1997.

[28]P.D. Thomas and C.K. Lombard , *Geometric conservation law and its application to flow computations on mvoing grids*, AIAA J. 17, 1979.

[29]M.R. Visbal and D. Gaitonde , *On the Use of High-Order Finite-Difference Schemes on Curvilinear and Deforming Meshes*, J. Comp. Phys., 181, 2002.

[30]J. Peraire and P.-O. Persson, *A Compact Discontinous Galerkin (CDG) method for Elliptic Problems*, in review SIAM J. of Scientific Computing., 2007

[31]P.-O. Persson and J. Peraire ,*An efficient low memory implicit DG algorithm for time dependent problems*, AIAA Paper 2006-0113, Reno, NV, 2006.

[32]P.-O. Persson, J. Peraire and J. Bonet, *Discontinuous Galerkin solution of the Navier-Stokes equations on deformable domains*, AIAA Paper 2007-0513, Reno, NV, 2007.

[33]B. Cockburn and C.-W. Shu, *The local discontinuous Galerkin method for time dependent convection-diffusion systems*, SIAM J. Numer. Anal., v35 (1998), pp.2440-2463.